Unique Surface Chemical Species on Indium Doped TiO_2 and Their Effect on the Visible Light Photocatalytic Activity

Enjun Wang,[†] Wensheng Yang,[‡] and Yaan Cao*,[†]

College of Physics, Nankai University, Tianjin 300071, P.R. China, and College of Chemistry, Jilin University, Changchun 130012, P.R. China

Received: May 5, 2009; Revised Manuscript Received: October 10, 2009

TiO_2 doped by different contents of indium was prepared by the sol−gel method by using titanium(IV) tetrabutoxide and indium chloride as precursors. It was revealed that a unique chemical species, $O-In-Cl_x$ ($x = 1$ or 2), existed on the surface of the indium doped TiO_2. The surface state energy level attributed to the surface $O-In-Cl_x$ species was located at 0.3 eV below the conduction band of TiO_2. The transition of electrons from the valence band of TiO_2 to the surface state energy level was responsive to visible light. The photogenerated carriers generated under visible light irradiation can be efficiently separated by the surface state energy level of the $O-In-Cl_x$ species and the valence band of TiO_2 to contribute to the photocatalytic reaction. Consequently, the indium doped TiO_2 showed improved photocatalytic activity for photodegradation of 4-chlorophenol compared to pure TiO_2 under visible light irradiation.

1. Introduction

TiO_2 photocatalyst has attracted much attention owing to its potential application in the solution of environmental pollution during the past decades.[1−3] However, TiO_2 is only sensitive to UV light due to its large band gap (3.0−3.2 eV) which results in a low efficiency to make use of solar light.[4,5] Recently, great attempts have been devoted to develop TiO_2-based photocatalysts sensitive to visible light in order to make use of solar energy much efficiently. Some strategies, such as surface modification,[6,7] metal or nonmetal ion doping,[8−12] generation of an oxygen vacancy,[13,14] combination with other semiconductors,[15,16] etc., have been widely adopted to prepare TiO_2 photocatalysts sensitive to visible light. Among these strategies, metal doped TiO_2 has been regarded as the second generation photocatalyst.[3] Various metal doped TiO_2's have been widely explored to improve the photocatalytic performance of TiO_2 on the degradation of various organic pollutants under visible light irradiation. For instance, Choi and co-workers reported that doping of TiO_2 with Fe^{3+}, Mo^{5+}, Ru^{3+}, Os^{3+}, Re^{5+}, V^{4+}, and Rh^{3+} at the 0.1−0.5% level increased the photocatalytic activity significantly, while Co^{3+} and Al^{3+} doping resulted in decreased photocatalytic activity.[1,17] Nagaveni et al. prepared the W^{3+}, V^{5+}, Ce^{4+}, Zr^{4+}, Fe^{3+}, and Cu^{2+} metal ion substituted nanocrystalline anatase TiO_2 and observed most of the metal ion doped TiO_2 showed higher photocatalytic activity than the commercial TiO_2 (Degussa P25) for photodegradation of 4-nitrophenol.[18] Our previous work proved that Sn^{4+} ion doped TiO_2 nanoparticle films prepared by the plasma-enhanced chemical vapor deposition method displayed a higher photocatalytic activity for photodegradation of phenol than pure TiO_2 under both UV and visible light.[11] Furthermore, the doping of TiO_2 with a variety of other metals such as La^{3+}, Pd^{2+}, Cr^{3+}, Ag^{+}, and rare earth ions (Sm^{3+}, Nd^{3+}, Pr^{3+}) has also been investigated by the researchers.[19−23] It is documented that the charge carrier recombination rates and interfacial electron-transfer rates of TiO_2 can be significantly affected by the concentration, energy level, and distribution of metal ion dopants.[3]

In recent years, $TiO_2-In_2O_3$ composite photocatalysts have been explored by many researchers.[24−28] Shchukin et al. prepared nanocrystalline bicomponent $TiO_2-In_2O_3$ powders with various Ti/In ratios by the sol−gel technique using indium(III) nitrate and $TiCl_4$ as precursors and evaluated their activity for photodegradation of 2-chlorophenol in water.[24] Poznyak et al. synthesized $TiO_2-In_2O_3$ composites by the sol−gel technique from concentrated hydrous titanium dioxide and indium hydroxide sols and studied their structures and optical and photoelectrochemical properties.[25] González and co-workers reported the synthesis, characterization, and photocatalytic properties of $In_2O_3-TiO_2$ catalysts.[26] Reddy et al. investigated the influence of In_2O_3 on the physicochemical properties of MoO_3/TiO_2 catalysts.[27] Yang and co-workers reported that the metallic silver and semiconductor indium oxide codoped titania nanocomposites ($Ag/In_2O_3-TiO_2$) showed enhanced photocatalytic activity.[28] Compared with pure TiO_2, the $In_2O_3-TiO_2$ composite photocatalysts showed an efficient separation of photogenerated carriers and an enhancement of photocatalytic activity under ultraviolet light irradiation.[24,26] However, the visible light photocatalytic activity of $TiO_2-In_2O_3$ composite photocatalysts has not been well explored up until now, possibly due to the large band gap of In_2O_3 (3.7 eV).[25]

In this work, the indium doped TiO_2 photocatalysts with response to visible light were prepared by the sol−gel technique by using $Ti(OC_4H_9)_4$ and $InCl_3$ as precursors. The experiments of 4-chlorophenol photocatalytic degradation showed that the indium doped TiO_2 photocatalysts presented higher photocatalytic activity than the pure TiO_2 and nitrogen doped TiO_2 under visible light irradiation. It was revealed that a unique surface chemical species, $O-In-Cl_x$ ($x = 1$ or 2), was formed on the surface of indium doped TiO_2. The surface state energy level in the band gap attributed to the $O-In-Cl_x$ species apparently improved the response of TiO_2 to visible light and promoted the efficient separation of the photogenerated electrons and holes. The mechanism for the improved photocatalytic activity

* To whom correspondence should be addressed. Phone: +86-22-66229598. E-mail: caoyaan@yahoo.com.
[†] Nankai University.
[‡] Jilin University.

10.1021/jp9041793
Published on Web 11/17/2009

of indium doped TiO_2 under visible light was discussed correspondingly.

2. Experimental Section

2.1. Catalyst Preparation. At room temperature, a certain volume of $InCl_3$ solution (0.6 mol/L) was mixed with 40 mL of anhydrous ethanol. After mixing, 12 mL of $Ti(OC_4H_9)_4$ was added dropwise to the solution under vigorous stirring. A concentrated HCl solution (12 mol/L) was added until the final pH of this mixture was about 3.5. The mixture was stirred continuously until the formation of TiO_2 gel. After aging at room temperature for 24 h, the as-prepared TiO_2 gel was dried at 100 °C, and then triturated to powder in an agate mortar. The powder was calcined at 450 °C for 2.5 h. A series of indium doped TiO_2 catalysts with different concentrations of indium was prepared by changing the volume of $InCl_3$ solution added in the ethanol. The catalysts were designated as $TiO_2-Inx\%$, where "*x*%" represents the nominal molar percentage content of In^{3+} ions in all metal ions (In^{3+} and Ti^{4+}) in TiO_2. Pure TiO_2 was prepared by the same procedure but by replacing the $InCl_3$ solution with deionized water. Nitrogen doped TiO_2 (TiO_2-N) was prepared by the hydrolysis of $Ti(OC_4H_9)_4$ in the presence of ammonia.[29]

2.2. Characterization. The XRD patterns were acquired on a Rigaku D/max 2500 X-ray diffraction spectrometer (Cu Kα, $\lambda = 1.54056$ Å). The average crystallite size was calculated according to the Scherrer formula ($D = k\lambda/B \cos\theta$). The BET surface areas of the samples were determined by nitrogen adsorption−desorption isotherm measurement at 77 K (Micromeritics Automatic Surface Area Analyzer Gemini 2360, Shimadzu). XPS measurements were carried out with an SECA Lab 220i-XL spectrometer by using an unmonochromated Al Kα (1486.6 eV) X-ray source. All of the spectra were calibrated to the binding energy of the adventitious C1s peak at 284.6 eV. Raman spectra were taken on a Bruker RFS 100/S Raman spectrometer by using the 1064 nm line of a Nd:YAG laser as the excitation source. The diffuse reflectance UV−visible absorption spectra were collected on a UV−visible spectrometer (U-4100, Hitachi). The photoluminescence (PL) spectra were measured by using the 340 nm line of a nanosecond Nd:YAG laser (NL303G) as the excitation source. The experimental setup consists of a spectrometer (Spex 1702), a photomultiplier tube (PMT, Hamamatsu R943), a lock-in amplifier, and a computer for data processing. All of the measurements were carried out at room temperature (25 ± 2 °C).

2.3. Evaluation of Photocatalytic Activity. The photocatalytic degradation of 4-chlorophenol was carried out in a 70 mL glass reactor with 10 mg amounts of catalysts suspended in 4-chlorophenol solution (5×10^{-5} mol L^{-1}, 40 mL, pH 5.74) under the visible light irradiation. A sunlamp (Philips HPA 400/30S, Belgium) was used as the light source, and a 400 nm filter was employed to remove ultraviolet light for obtainment of visible light. The reactor was perpendicular to the light beam and located 10 cm away from the light source. The 4-chlorophenol solution was continuously bubbled by O_2 gas at a flux of 5 mL min^{-1} under magnetic stirring at 25 ± 2 °C. Every 2 h, the residual concentration of 4-chlorophenol was measured by a UV−visible spectrometer (UV-1061PC, SHIMADZU) by using 4-aminoantipyrine as the chromogenic reagent. Prior to photocatalytic reactions, the suspension was magnetically stirred in the dark for 30 min, which was enough to reach the adsorption equilibrium of 4-chlorophenol. The reproducibility of the photocatalytic degradation was evaluated by repeating the experiments at least three times with different batches of the photocatalysts prepared by the same procedure. The blank experiment was performed under identical conditions. Deionized water (18.2 MΩ·cm) was used in all of the experiments, and the chemicals were all of analytical grade.

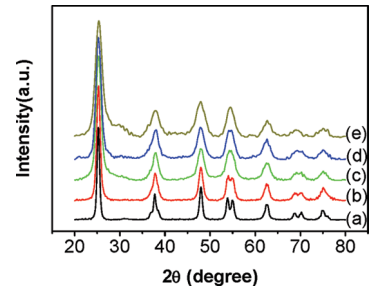

Figure 1. XRD patterns of pure TiO_2 (a), $TiO_2-In3\%$ (b), $TiO_2-In7\%$ (c), $TiO_2-In10\%$ (d), and $TiO_2-In15\%$ (e).

TABLE 1: Cell Parameters, Crystallite Size, and Specific Surface Area of Pure TiO_2 and $TiO_2-Inx\%$ Samples

sample	cell parameters (Å) $a = b$	cell parameters (Å) c	cell volume (Å^3)	crystallite size (nm)	S_{BET} ($m^2\ g^{-1}$)
TiO_2	3.788	9.516	136.5	12.6	68
$TiO_2-In3\%$	3.782	9.524	136.2	8.8	76
$TiO_2-In7\%$	3.782	9.535	136.4	6.2	112
$TiO_2-In10\%$	3.779	9.518	135.9	6.0	110
$TiO_2-In15\%$	3.782	9.535	136.4	4.9	114

3. Results and Discussion

3.1. Structure of the Indium Doped TiO_2. Figure 1 shows X-ray diffraction spectra of pure TiO_2, $TiO_2-In3\%$, $TiO_2-In7\%$, $TiO_2-In10\%$, and $TiO_2-In15\%$. The pure TiO_2 (curve a) exhibited an anatase structure.[29] The position and shape of the diffractive peaks of $TiO_2-Inx\%$ (curves b−e) were quite similar to those of TiO_2 (curve a), indicating after doping the crystalline phase of anatase TiO_2 was not changed. Except for the diffraction peaks of anatase, a weak peak at around 30.5° was observed in $TiO_2-In15\%$ (curve e), which indicated the presence of a small amount of In_2O_3.[30] No characteristic diffractive peaks of other indium species, such as $InCl_3$, were observed in the $TiO_2-Inx\%$ (curves b−e). The diffraction peak of crystal planes (101) was selected to estimate the crystal size of all samples by the Debye−Scherrer equation.[31] The results indicated that the crystallite size of the catalysts decreased gradually with an increase of the doping content of indium ions. At the same time, their specific surface area (BET) increased gradually, as shown in Table 1.

It is documented that there are two kinds of doping modes, interstitial and substitutional, for doped metal ions in oxides.[11] In the case of the interstitial mode, the ionic radius of dopant should be smaller than that of the lattice metal ion and the oxide lattice spacing, allowing the doping metal ions to enter into the crystal cell of the oxide. The ionic radius of the doping In^{3+} ion (81 pm)[32] is larger than that of the lattice Ti^{4+} ion (53 pm);[11] it is impossible for the In^{3+} ions to enter into the crystal cell of TiO_2 through the interstitial mode. Upon doping through the substitutional mode, the doping metal ions will substitute the lattice metal ions and thus occupy the positions of the lattice metal ions in the oxide. If the ionic radius of the doping ions is larger than that of the lattice ions, the lattice parameters and cell volume of the doped oxide should be larger than those of the pure oxide. As a result, the positions of all of the diffraction peaks in XRD patterns should shift to lower diffraction angles. It is seen that no shift of the peaks was observable in the XRD patterns of the indium doped TiO_2, as shown in Figure 1, and

TABLE 2: Peak Positions (eV) and Assignments of the Pure TiO_2 and TiO_2−In*x*% Samples

	O1s	Ti2p		In3d		Cl2p	
sample	lattice O^{2-}	$Ti2p_{3/2}$	$Ti2p_{1/2}$	$In3d_{5/2}$	$In3d_{3/2}$	$Cl2p_{3/2}$	$Cl2p_{1/2}$
TiO_2	529.5	458.3	464.0			198.2	199.9
TiO_2−In3%	529.8	458.5	464.2	444.8	452.4	198.6	200.2
TiO_2−In7%	530.0	458.7	464.4	445.2	452.8	198.5	200.1
TiO_2−In10%	530.0	458.6	464.3	445.1	452.7	198.6	200.3
TiO_2−In15%	529.8	458.5	464.2	445.3	452.9	198.5	200.2

the lattice parameters and cell volume of TiO_2−In*x*% samples were almost the same as those of pure TiO_2 (see Table 1). Therefore, the doping of In^{3+} ions into TiO_2 through the substitutional mode can also be excluded. Thus, it is reasonable to suppose that the In^{3+} ions are doped on the surface of TiO_2.

3.2. Surface Chemical Structure of the Doped TiO_2. XPS measurements were carried out to investigate the chemical states of all of the elements in the pure TiO_2 and TiO_2−In*x*% samples. Except for C, O, Ti, In, and Cl, no other elements were detected in the samples. The peak positions of all of the elements in TiO_2 and TiO_2−In*x*% samples are illustrated in Table 2. For the pure TiO_2, the peak of $Cl2p_{3/2}$ at 198.2 eV is the same as that of $Cl2p_{3/2}$ in $TiCl_4$ (198.2 eV),[33] which is assigned to the Cl^- ions linked with Ti^{4+}. Since the ionic radius of Cl^- ion is larger than that of O^{2-} (1.81 Å versus 1.40 Å), lattice O^{2-} in TiO_2 cannot be substituted by Cl^- during the reactions.[34] Thus, it is deduced that the Cl^- ions should be located on the TiO_2 surface via the coordination with the unsaturated Ti^{4+} sites.

Figure 2a shows the In3d XPS spectra of TiO_2−In*x*% samples. The peaks at 444.8−445.3 eV and 452.4−452.9 eV are assigned to In $3d_{5/2}$ and In $3d_{3/2}$, respectively. The binding energies of In $3d_{5/2}$ (444.8−445.3 eV) in TiO_2−In*x*% samples are located between those of In $3d_{5/2}$ in In_2O_3 (444.6 eV)[27] and In $3d_{5/2}$ in $InCl_3$ (446.0 eV).[35] In the Cl 2p XPS spectra of TiO_2−In*x*% (see Figure 2b), the binding energies of $Cl2p_{3/2}$ are identified to be 198.5−198.6 eV, which are located between those of Cl $2p_{3/2}$ in $TiCl_4$ (198.2 eV)[33] and Cl $2p_{3/2}$ in $InCl_3$ (199.1 eV).[35] These results suggest that the In^{3+} ions link with the unsaturated oxygen and Cl^- ions, respectively, thus meaning the formation of O−In−Cl_x ($x = 1$ or 2) structure on the surface of TiO_2−In*x*%. A part of the Cl^- ions may also link with the unsaturated Ti to form the O−Ti−Cl structure. Raman spectra were recorded to further investigate the formation of the surface species (Figure 3). All of the samples show characteristic bands at 142, 195, 395, 515, and 637 cm^{-1}, which are assigned to the E_g, B_{1g}, A_{1g}, B_{2g}, and E_g vibrational modes of TiO_2, respectively, indicating the presence of the anatase phase in all of these samples.[29] Except these peaks, some additional peaks around 300, 470, and 618 cm^{-1} were observed for the TiO_2−In7% and TiO_2−In10% samples. Gómez et al. have reported that three peaks at 288, 467, and 608 cm^{-1} were observed in the Raman spectrum of In_2O_3.[26] Therefore, we ascribed these peaks to the vibrational modes of In−O bonds. Furthermore, in comparison to the Raman peak of $InCl_3$ at 280 cm^{-1}, the peaks around 275 cm^{-1} are supposed to be related to the In−Cl.[36] The Raman spectra suggested the existence of both In−O and In−Cl bonds as the surface chemical species of the In doped TiO_2, which is consistent with the results of XPS that O−In−Cl_x was formed on the surface of the doped TiO_2.

On the basis of the above experimental results and discussion, we proposed a mechanism for the formation of surface species in the doped TiO_2 (Scheme 1). In the sol−gel process, the TiO_2 could rapidly precipitate at a pH of 3.5 and $InCl_3$ could only be partially hydrolyzed. Thus, some In species, such as $InCl_3$, $InCl_2OH$, and $InCl(OH)_2$, may be absorbed on the surface of TiO_2. It is expected that these species would link with the unsaturated oxygen on the surface of TiO_2 to form the O−In−Cl_x structure and some Cl ions would link with the unsaturated Ti to form the O−Ti−Cl structure during the subsequent calcination process.

Pure TiO_2 shows Ti2p peaks assigned to Ti $2p_{3/2}$ and Ti $2p_{1/2}$ at 458.3 and 464.0 eV (Figure 4) and an O1s peak assigned to lattice O^{2-} at 529.5 eV (Figure 5).[37] In the case of TiO_2−In*x*% samples, all of the peaks of Ti2p and O1s of TiO_2 present higher binding energies after the doping of In^{3+}, which is consistent with the formation of O−In−Cl_x structure on the TiO_2 surface after the doping. The Pauling electronegativity of In^{3+} ion (1.7) in the Ti−O−In−Cl_x structure is larger than that of the Ti^{4+} ion (1.5) in the Ti−O−Ti structure,[27] which will induce the possible electron transfer from Ti^{4+} and O^{2-} to In^{3+} in the Ti−O−In−Cl_x structure. Such a charge transfer will make Ti^{4+} and O^{2-} be poorer in electrons and thus result in an increase in the binding energies of Ti 2p and O 1s core electrons. It is noted that, in Figure 5, the O 1s signals present shoulders located at the side of higher binding energy, which are assigned to the OH species on the surface.[38] It is clear that the amount of the

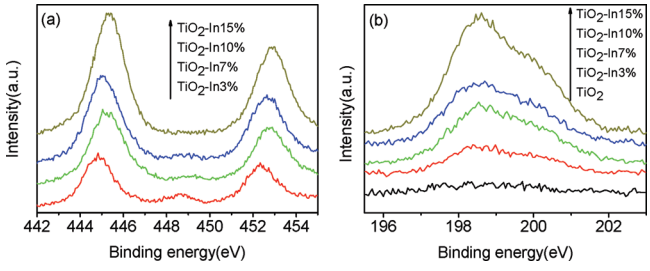

Figure 2. In 3d (a) XPS spectra of TiO_2−In*x*%; Cl 2p (b) XPS spectra of TiO_2 and TiO_2−In*x*%.

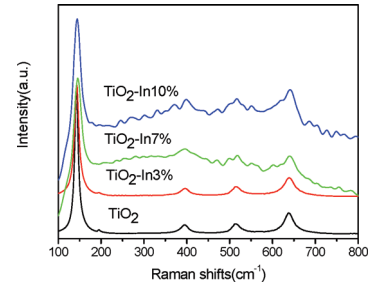

Figure 3. Raman spectra of the pure TiO_2 and TiO_2−In*x*%.

SCHEME 1: Proposed Mechanism for the Formation of Surface Species ($x = 1$ or 2)

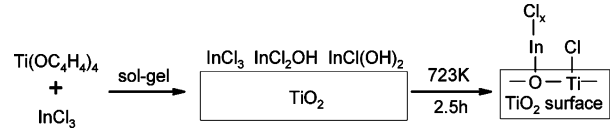

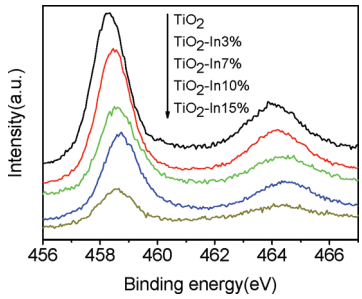

Figure 4. Ti2p XPS spectra of pure TiO_2 and $TiO_2-Inx\%$.

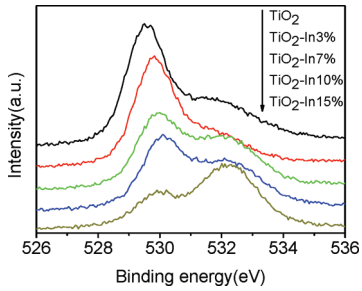

Figure 5. O1s XPS spectra of pure TiO_2 and $TiO_2-Inx\%$.

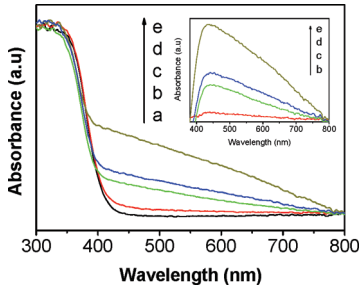

Figure 6. Diffuse reflectance UV−visible spectra of pure TiO_2 (a), $TiO_2-In3\%$ (b), $TiO_2-In7\%$ (c), $TiO_2-In10\%$ (d), and $TiO_2-In15\%$ (e). The inset gives the difference DRS spectra of $TiO_2-Inx\%$ (curves b−e).

hydroxyl groups on the TiO_2 surface increased greatly after being doped by indium.

3.3. Response of the Doped TiO_2 to Visible Light. The diffuse reflectance UV−visible absorption spectra of pure TiO_2 and $TiO_2-Inx\%$ samples are given in Figure 6. The pure TiO_2 (curve a) shows a strong peak at 350 nm, which is attributed to the electronic transition from the valence band to the conduction band of TiO_2.[29] The band threshold at 400 nm corresponds to a band gap of 3.1 eV. For $TiO_2-Inx\%$ samples, absorption peaks at 350 nm attributed to the transition of band−band of TiO_2 have almost no shift compared with pure TiO_2 (curves b−e), indicating after the doping of indium ions the band gaps of $TiO_2-Inx\%$ samples are not changed. In addition, a broad absorption in the range of wavelengths from 400 to 800 nm is observed in $TiO_2-Inx\%$ samples. The difference DRS spectra were obtained by subtracting the absorbance spectra of pure TiO_2 (curve a) from the spectra of $TiO_2-Inx\%$ (curves b−e) in Figure 6,[39−42] which is shown in the inset in Figure 6. The position of the absorption maximum was around 440 nm, corresponding to an energy level gap of about 2.8 eV. Moreover, the intensity of absorption in the visible region increased with the increased content of In^{3+} ions doped in TiO_2 (curves b−e, the inset in Figure 6). It is deduced that the remarkable absorption at 400−800 nm is related to the doped In^{3+} ions. According to the analyses of XPS, after doping In^{3+} ions into TiO_2, the $O-In-Cl_x$ and O−Ti−Cl species existed on the

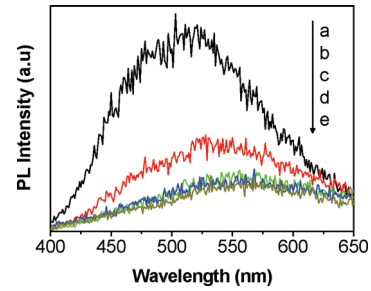

Figure 7. Photoluminescence spectra of pure TiO_2 (a), $TiO_2-In3\%$ (b), $TiO_2-In7\%$ (c), $TiO_2-In10\%$ (d), and $TiO_2-In15\%$ (e).

surface of $TiO_2-Inx\%$ samples. In order to make clear what species are responsible for the visible light absorption of the doped TiO_2, the surface of pure TiO_2 was treated with concentrated HCl to replace the surface OH groups of TiO_2 with Cl^-, which resulted in the formation of O−Ti−Cl species. However, there is no difference between the absorption spectra of pure TiO_2 and the treated TiO_2 samples (see Figure S1 in the Supporting Information). Thus, it is reasonable to attribute the visible light absorption to $O-In-Cl_x$ species on the surface of the doped TiO_2. The surface state energy level contributed by the $O-In-Cl_x$ species is likely to locate at about 0.3 eV below the conduction band of TiO_2, which is further supported by the laser photoluminescence spectral measurements in the following part. The absorption peak at 400−800 nm was ascribed to the electronic transition from the valence band of TiO_2 to the surface state energy level of the $O-In-Cl_x$ species.

3.4. Photoluminescence Spectra. Figure 7 shows the PL emission spectra of pure TiO_2 and $TiO_2-Inx\%$ samples. Two peaks around 480 and 525 nm are observed for the pure TiO_2 (Figure 7a), attributed to the transition from the oxygen vacancies with two trapped electrons and one trapped electron to the valence band of TiO_2, respectively.[43−46] The energy levels related to the two kinds of the oxygen vacancies are located at 0.51[44] and 0.82 eV[46] below the conduction band of TiO_2, respectively. Due to the existence of the energy levels of oxygen vacancies, first the photogenerated electrons in the conduction band should reach the oxygen vacancies through a nonirradiative process, and then recombine with the photogenerated holes in the valence band accompanied by the emission of fluorescence. It can be seen that the emission intensity of TiO_2 is weakened significantly in $TiO_2-Inx\%$ (Figure 7b−e), indicating that the recombination of photogenerated carriers via transition from the oxygen vacancies to the valence band of TiO_2 is suppressed effectively upon the doping of In^{3+} ions. This observation further suggested that the surface state energy level attributed to the $O-In-Cl_x$ species on the surface of $TiO_2-Inx\%$ should locate between the conduction band of $TiO_2-Inx\%$ and the energy level of oxygen vacancies, which is also consistent with the UV−visible absorption spectra. Since the surface state energy level of $O-In-Cl_x$ species which located at 0.3 eV below the conduction band in $TiO_2-Inx\%$ samples was higher than those of oxygen vacancies (0.51 and 0.82 eV below the conduction band), the photogenerated electrons from the conduction band prefer to move from the conduction band of TiO_2 to the surface state energy level rather than to the oxygen vacancies. As a result, the photogenerated electrons and holes tend to accumulate on the surface state energy level of TiO_2 and at the valence band of TiO_2, respectively. Thus, the emission intensity of TiO_2 originated from the transition from the oxygen vacancies to the valence band of TiO_2 decreased greatly after being doped by In^{3+} ions.

TABLE 3: Photodegradation of 4-Chlorophenol (4-CP) under Visible Light Irradiation ($\lambda > 400$ nm)

sample	4-CP degraded,[a] $(c_0 - c)/c_0$ (%)	k^b (min^{-1})	$t_{1/2}$ (min)	specific photocatalytic activity (mol g^{-1} h^{-1})
blank[c]	5.2 ± 0.2	$(1.13 \pm 0.02) \times 10^{-4}$	$(6.10 \pm 0.07) \times 10^3$	
TiO_2	8.2 ± 0.5	$(1.72 \pm 0.04) \times 10^{-4}$	$(3.92 \pm 0.11) \times 10^3$	$(2.05 \pm 0.13) \times 10^{-6}$
TiO_2-N	21.9 ± 2.2	$(5.17 \pm 0.68) \times 10^{-4}$	$(1.34 \pm 0.14) \times 10^3$	$(5.48 \pm 0.55) \times 10^{-6}$
$TiO_2-In3\%$	18.0 ± 2.1	$(3.90 \pm 0.54) \times 10^{-4}$	$(1.79 \pm 0.23) \times 10^3$	$(4.51 \pm 0.52) \times 10^{-6}$
$TiO_2-In7\%$	38.8 ± 3.7	$(1.02 \pm 0.14) \times 10^{-3}$	$(6.47 \pm 0.84) \times 10^2$	$(9.68 \pm 0.92) \times 10^{-6}$
$TiO_2-In10\%$	37.8 ± 3.5	$(9.69 \pm 1.32) \times 10^{-4}$	$(7.12 \pm 0.88) \times 10^2$	$(9.45 \pm 0.87) \times 10^{-6}$
$TiO_2-In15\%$	31.6 ± 2.9	$(7.88 \pm 0.97) \times 10^{-4}$	$(8.78 \pm 0.78) \times 10^2$	$(7.90 \pm 0.74) \times 10^{-6}$

[a] After reaction for 8 h. [b] Apparent rate constant deduced from the linear fitting of $\ln(c_0/c)$ versus reaction time. [c] The blank was the photolysis of 4-chlorophenol.

3.5. Photocatalytic Activity. The photodegradation of 4-chlorophenol was employed to evaluate the photocatalytic activities of pure TiO_2, nitrogen doped TiO_2, and $TiO_2-Inx\%$ samples, and the experimental results of the photodegradation under visible light ($\lambda > 400$ nm) are illustrated in Table 3. The $\ln(C_0/C)$ values of 4-chlorophenol show a linear correlation with photodegradation time, suggesting a first-order reaction for all samples. It is shown that 4-chlorophenol is scarcely photodegraded in the blank experiment. The pure TiO_2 photocatalyst shows a low photocatalytic activity; only 8.2% of 4-chlorophenol was decomposed in the pure TiO_2 suspension after 8 h. The $TiO_2-Inx\%$ catalysts show an improved photocatalytic activity under visible light. The highest activity is observed in the $TiO_2-In7\%$ sample, in which 38.8% of 4-chlorophenol was degraded after 8 h of visible light irradiation. The photodegraded rate and the specific photocatalytic activity of $TiO_2-In7\%$ are about 4 times those of pure TiO_2. It is more significant that the photocatalytic activity of the $TiO_2-In7\%$ sample is about 2 times that of nitrogen doped TiO_2. It is confirmed that indium doping is an effective way of preparing a visible-light-activated TiO_2 photocatalyst.

It is hard to excite pure TiO_2 by the visible light due to its large band gap (3.1 eV), which would induce a low photocatalytic activity for photodegradation of 4-chlorophenol. The doping of indium ions resulted in the formation of the surface state energy level originated from the $O-In-Cl_x$ species on $TiO_2-Inx\%$ samples, and the appearance of the broad absorption at 400−800 nm attributed to the electronic transition from the valence band of TiO_2 to the surface state energy level. As a result, photogenerated electrons and holes can be directly and efficiently separated on the surface of TiO_2 under the visible light irradiation. The photogenerated electrons tend to accumulate at the surface state energy level, and the photogenerated holes are collected at the valence band of TiO_2 on the surface. During the photocatalytic reaction, 4-chlorophenol molecules adsorbed in the surface active sites on $TiO_2-Inx\%$ are immediately oxidized by photogenerated holes from the valence band of the catalyst. At the same time, the photogenerated electrons accumulated at the surface state energy level which is higher than the electrode potential of O_2/H_2O_2 (NHE 0.34 eV) can be captured directly by the efficiently adsorbed O_2 molecules on the surface of $TiO_2-Inx\%$ to form O_2^- active species for further photodecomposition of the 4-chlorophenol molecules.[11] The recombination of photogenerated carriers originated from the transition from the oxygen vacancies to the valence band of TiO_2 also decreased greatly, since the surface state energy level of $O-In-Cl_x$ species located at 0.3 eV below the conduction band in $TiO_2-Inx\%$ samples was higher than those of oxygen vacancies (0.51 and 0.82 eV below the conduction band). Although the increased amount of hydroxyl (OH) groups and bridging oxygen on $TiO_2-Inx\%$ samples and increased surface area of the catalysts upon indium doping may also contribute to the improved photcatalytic activity, the formation of the surface species $O-In-Cl_x$ is the primary reason for the enhanced visible light photocatalytic activity, since the 4-chlorophenol cannot be decomposed by the TiO_2 under the visible light irradiation without the generation and separation of photoinduced charge carriers under visible light.

It should be noted that the photocatalytic activity of $TiO_2-Inx\%$ decreased when the content of the indium loaded exceeded 10 mol %, although the intensity of visible light absorption increased. This should be attributed to the formation of In_2O_3 at the higher content of indium, as indicated in Figure 1, which will cover the surface of the catalyst and retard the charge transfer from the indium doped catalysts to O_2 or 4-chlorophenol molecules.[29,47]

4. Conclusion

A new kind of TiO_2-based visible light photocatalysts with a surface chemical structure of $O-In-Cl_x$ was successfully prepared by doping of indium ions. The photocatalysts present higher photocatalytic activity than pure TiO_2 and nitrogen doped TiO_2 under visible light irradiation. The surface state energy level located at 0.3 eV below the conduction band attributed to the $O-In-Cl_x$ species on the TiO_2 surface allowed the more efficient utilization of visible light, and promoted the direct separation of photogenerated carriers. It is expected that the more precise control over the surface structure should be helpful for the development of the doped TiO_2 photocatalyst with better performance under visible light.

Acknowledgment. This work was supported by National Natural Science Foundation of China (Nos. 20573060 and 50872056).

Supporting Information Available: Diffuse reflectance UV−vis spectra of TiO_2 and HCl treated TiO_2. This material is available free of charge via the Internet at http://pubs.acs.org.

References and Notes

(1) Choi, W.; Termin, A.; Hoffmann, M. R. *J. Phys. Chem.* **1994**, *98*, 13669.
(2) Ghicov, A.; Macak, J. M.; Tsuchiya, H.; Kunze, J.; Haeublein, V.; Frey, L.; Schmuki, P. *Nano Lett.* **2006**, *6*, 1080.
(3) Chen, X.; Mao, S. S. *Chem. Rev.* **2007**, *107*, 2891.
(4) Hoffmann, M. R.; Martin, S. T.; Choi, W.; Bahnemann, D. W. *Chem. Rev.* **1995**, *95*, 69.
(5) Ding, Z.; Lu, G. Q.; Greenfield, P. F. *J. Phys. Chem. B* **2000**, *104*, 4815.
(6) Kisch, H.; Zang, L.; Lange, C.; Maier, W. F.; Antonius, C.; Meissner, D. *Angew. Chem., Int. Ed. Engl.* **1998**, *37*, 3034.
(7) Zang, L.; Macyk, W.; Lange, C.; Maier, W. F.; Antonius, C.; Meissner, D.; Kish, H. *Chem.—Eur. J.* **2000**, *6*, 379.
(8) Chang, S.; Doong, R. *J. Phys. Chem. B* **2006**, *110*, 20808.
(9) Chen, D.; Jiang, Z.; Geng, J.; Wang, Q.; Yang, D. *Ind. Eng. Chem. Res.* **2007**, *46*, 2741.

(10) Cong, Y.; Zhang, J.; Chen, F.; Anpo, M.; He, D. *J. Phys. Chem. C* **2007**, *111*, 10618.
(11) Cao, Y.; Yang, W.; Zhang, W.; Liu, G.; Yue, P. *New J. Chem.* **2004**, *28*, 218.
(12) Luo, H.; Takata, T.; Lee, Y.; Zhao, J.; Domen, K.; Yan, Y. *Chem. Mater.* **2004**, *16*, 846.
(13) Justicia, I.; Ordejon, P.; Canto, G.; Mozos, J. L.; Fraxedas, J.; Battiston, G. A.; Gerbasi, R.; Figueras, A. *Adv. Mater.* **2002**, *14*, 1399.
(14) Nakamura, I.; Negishi, N.; Kutsuna, S.; Ihara, T.; Sugihara, S.; Takeuchi, K. *J. Mol. Catal. A* **2000**, *161*, 205.
(15) Marcì, G.; Augugliaro, V.; Muñoz, M. J. L.; Martń, C.; Palmisano, L.; Rives, V.; Schiavello, M.; Tilley, R. J. D.; Venezia, A. M. *J. Phys. Chem. B* **2001**, *105*, 1026.
(16) Mishra, T. *Catal. Commun.* **2008**, *9*, 21.
(17) Choi, W.; Termin, A.; Hoffmann, M. R. *Angew. Chem.* **1994**, *106*, 1148.
(18) Nagaveni, K.; Hegde, M. S.; Madras, G. *J. Phys. Chem. B* **2004**, *108*, 20204.
(19) Huo, Y.; Zhu, J.; Li, J.; Li, G.; Li, H. *J. Mol. Catal. A* **2007**, *278*, 237.
(20) Wu, C.; Chao, C.; Kuo, F. *Catal. Today* **2004**, *97*, 103.
(21) Anpo, M.; Takeuchi, M. *J. Catal.* **2003**, *216*, 505.
(22) Wang, P.; Wang, D.; Xie, T.; Li, H.; Yang, M.; Wei, X. *Mater. Chem. Phys.* **2008**, *109*, 181.
(23) Liang, C.; Li, F.; Liu, C.; Lu, J.; Wang, X. *Dyes Pigm.* **2008**, *76*, 477.
(24) Shchukin, D.; Poznyak, S.; Kulak, A.; Pichat, P. *J. Photochem. Photobiol., A* **2004**, *162*, 423.
(25) Poznyak, S. K.; Talapin, D. V.; Kulak, A. I. *J. Phys. Chem. B* **2001**, *105*, 4816.
(26) González, V. R.; Rodrǵuez, A. M.; May, M.; Tzompantzi, F.; Gómez, R. *J. Photochem. Photobiol., A* **2008**, *193*, 266.
(27) Reddya, B. M.; Chowdhury, B.; Smirniotis, P. G. *Appl. Catal., A* **2001**, *219*, 53.
(28) Yang, X.; Wang, Y.; Xu, L.; Yu, X.; Guo, Y. *J. Phys. Chem. C* **2008**, *112*, 11481.
(29) Gao, B.; Ma, Y.; Cao, Y.; Yang, W.; Yao, J. *J. Phys. Chem. B* **2006**, *110*, 14391.
(30) Reddy, B. M.; Ganesh, I.; Khan, A. *Appl. Catal., A* **2003**, *248*, 169.
(31) Surolia, P. K.; Tayade, R. J.; Jasra, R. V. *Ind. Eng. Chem. Res.* **2007**, *46*, 6196.
(32) Okushita, H.; Shimidzu, T. *Bull. Chem. Soc. Jpn.* **1990**, *63*, 920.
(33) Mousty-Desbuquoit, C.; Riga, J.; Verbist, J. J. *J. Chem. Phys.* **1983**, *79*, 26.
(34) Zhu, J.; Zheng, W.; He, B.; Zhang, J.; Anpo, M. *J. Mol. Catal. A* **2004**, *216*, 35.
(35) Freeland, B. H.; Habeeb, J. J.; Tuck, D. G. *Can. J. Chem.* **1977**, *55*, 1528.
(36) The Raman Spectra Database of Minerals and Inorganic Materials, http://riodb.ibase.aist.go.jp/db092/cgi-bin/inorganic_search.pl?lang=E&name=&Atom_O=ON&Atom_In=ON.
(37) Cao, Y.; Meng, Q.; Yang, W.; Yao, J.; Shu, Y.; Wang, W.; Chen, G. *Colloids Surf., A* **2005**, *262*, 181.
(38) Erdem, B.; Hunsicker, R. A.; Simmons, G. W.; Sudol, E. D.; Dimonie, V. L.; El-Aasser, M. S. *Langmuir* **2001**, *17*, 2664.
(39) Kuznetsov, V. N.; Malkin, M. G. *J. Appl. Spectrosc.* **2000**, *67*, 763.
(40) Kuznetsov, V. N.; Serpone, N. *J. Phys. Chem. B* **2006**, *110*, 25203.
(41) Serpone, N. *J. Phys. Chem. B* **2006**, *110*, 24287.
(42) Qiu, X.; Zhao, Y.; Burda, C. *Adv. Mater.* **2007**, *19*, 3995.
(43) Li, D.; Haneda, H.; Hishita, S.; Ohashi, N. *Chem. Mater.* **2005**, *17*, 2596.
(44) Serpone, N.; Lawless, D.; Khairutdinov, R. *J. Phys. Chem.* **1995**, *99*, 16655.
(45) Yu, J. C.; Ho, W.; Yu, J.; Hark, S. K.; Iu, K. *Langmuir* **2003**, *19*, 3889.
(46) Saraf, L. V.; Patil, S. I.; Ogale, S. B.; Sainkar, S. R.; Kshirsager, S. T. *Int. J. Mod. Phys. B* **1998**, *12*, 2635.
(47) Tada, H.; Kokubu, A.; Iwasaki, M.; Ito, S. *Langmuir* **2004**, *20*, 4665.

JP9041793